

DRAFT VERSION FEBRUARY 9, 2024  
Typeset using L<sup>A</sup>T<sub>E</sub>X **modern** style in AASTeX631

## UNCOVER: JWST Spectroscopy of Three Cold Brown Dwarfs at Kiloparsec-scale Distances

ADAM J. BURGASSER,<sup>1</sup> RACHEL BEZANSON,<sup>2</sup> IVO LABBE,<sup>3</sup> GABRIEL BRAMMER,<sup>4</sup>  
SAM E. CUTLER,<sup>5</sup> LUKAS J. FURTAK,<sup>6</sup> JENNY E. GREENE,<sup>7</sup> ROMAN GERASIMOV,<sup>8,9</sup>  
JOEL LEJA,<sup>10,11,12</sup> RICHARD PAN,<sup>13</sup> SEDONA H. PRICE,<sup>2</sup>  
BINGJIE WANG (王冰洁),<sup>10,11,12</sup> JOHN R. WEAVER,<sup>5</sup> KATHERINE E. WHITAKER,<sup>5,14</sup>  
SEIJI FUJIMOTO,<sup>15,\*</sup> VASILY KOKOREV,<sup>16</sup> PRATIKA DAYAL,<sup>16</sup>  
THEMIYA NANAYAKKARA,<sup>17</sup> CHRISTINA C. WILLIAMS,<sup>18</sup> DANILO MARCHESINI,<sup>19</sup>  
ADI ZITRIN,<sup>20</sup> AND PIETER VAN DOKKUM<sup>†</sup>

<sup>1</sup>*Department of Astronomy & Astrophysics, UC San Diego, La Jolla, CA 92093, USA*

<sup>2</sup>*Department of Physics and Astronomy and PITT PACC, University of Pittsburgh, Pittsburgh, PA 15260, USA*

<sup>3</sup>*Centre for Astrophysics and Supercomputing, Swinburne University of Technology, Melbourne, VIC 3122, Australia*

<sup>4</sup>*Cosmic Dawn Center (DAWN), Niels Bohr Institute, University of Copenhagen, Jagtvej 128, København N, DK-2200, Denmark*

<sup>5</sup>*Department of Astronomy, University of Massachusetts, Amherst, MA 01003, USA*

<sup>6</sup>*Physics Department, Ben-Gurion University of the Negev, P.O. Box 653, Be'er-Sheva 84105, Israel*

<sup>7</sup>*Department of Astrophysical Sciences, Princeton University, 4 Ivy Lane, Princeton, NJ 08544*

<sup>8</sup>*Department of Physics, UC San Diego, La Jolla, CA 92093, USA*

<sup>9</sup>*Department of Physics & Astronomy, University of Notre Dame, Notre Dame, IN 46556, USA*

<sup>10</sup>*Department of Astronomy & Astrophysics, The Pennsylvania State University, University Park, PA 16802, USA*

<sup>11</sup>*Institute for Computational & Data Sciences, The Pennsylvania State University, University Park, PA 16802, USA*

<sup>12</sup>*Institute for Gravitation and the Cosmos, The Pennsylvania State University, University Park, PA 16802, USA*

<sup>13</sup>*Department of Physics and Astronomy, Tufts University, 574 Boston Ave., Medford, MA 02155, USA*

<sup>14</sup>*Cosmic Dawn Center (DAWN), Denmark*

<sup>15</sup>*Department of Astronomy, The University of Texas at Austin, Austin, TX 78712, USA*

<sup>16</sup>*Kapteyn Astronomical Institute, University of Groningen, 9700 AV Groningen, The Netherlands*

<sup>17</sup>*Centre for Astrophysics and Supercomputing, Swinburne University of Technology, PO Box 218, Hawthorn, VIC 3122, Australia*

<sup>18</sup>*NSF's National Optical-Infrared Astronomy Research Laboratory, 950 N. Cherry Avenue, Tucson, AZ 85719, USA*

<sup>19</sup>*Department of Physics & Astronomy, Tufts University, MA 02155, USA*

<sup>20</sup>*Physics Department, Ben-Gurion University of the Negev, P.O. Box 653, Be'er-Sheva 84105, Israel*

(Accepted 22 Nov 2023)

Corresponding author: Adam Burgasser  
aburgasser@ucsd.edu

## ABSTRACT

We report JWST/NIRSpec spectra of three distant T-type brown dwarfs identified in the Ultradeep NIRSpec and NIRCам ObserVations before the Epoch of Reionization (UNCOVER) survey of the Abell 2744 lensing field. One source was previously reported as a candidate T dwarf on the basis of NIRCам photometry, while two sources were initially identified as candidate active galactic nuclei. Low-resolution 1–5  $\mu\text{m}$  spectra confirm the presence of molecular features consistent with T dwarf atmospheres, and comparison to spectral standards infers classifications of sdT1, T6, and T8–T9. The warmest source, UNCOVER-BD-1, shows evidence of subsolar metallicity, and atmosphere model fits indicates  $T_{\text{eff}} = 1300$  K and  $[\text{M}/\text{H}] \sim -1.0$ , making this one of the few spectroscopically-confirmed T subdwarfs known. The coldest source, UNCOVER-BD-3, is near the T/Y dwarf boundary with  $T_{\text{eff}} = 550$  K, and our analysis indicates the presence of  $\text{PH}_3$  in the 3–5  $\mu\text{m}$  region, favored over  $\text{CO}_2$  and a possible indicator of subsolar metallicity. We estimate distances of 0.9–4.5 kpc from the Galactic midplane, making these the most distant brown dwarfs with spectroscopic confirmation. Population simulations indicate high probabilities of membership in the Galactic thick disk for two of these brown dwarfs, and potential halo membership for UNCOVER-BD-1. Our simulations indicate that there are approximately 5 T dwarfs and 1–2 L dwarfs in the Abell 2744 field down to  $F444W = 30$  AB mag, roughly one-third of which are thick disk members. These results highlight the utility of deep JWST/NIRSpec spectroscopy for identifying and characterizing the oldest metal-poor brown dwarfs in the Milky Way.

*Keywords:* Brown dwarfs (185), T dwarfs (1679), T subdwarfs (1680), Milky Way stellar halo (1060), Sky surveys (1464)

## 1. INTRODUCTION

Brown dwarfs are stellar objects with masses below the  $\sim 0.075 M_{\odot}$  threshold for sustained core hydrogen fusion (Kumar 1962, 1963; Hayashi & Nakano 1963). Supported by electron degeneracy pressure, these compact, hydrogen-rich objects radiate their initial heat of formation and continuously cool over time. The relatively high abundance of brown dwarfs in the immediate vicinity of the Sun ( $\gtrsim 20\%$  of stars; Kirkpatrick et al. 2021; Reyl   et al. 2021), their lack of chemical processing, and their time-dependent luminosities make them useful probes of the ages and chemical evolution of various Milky Way populations (Stauffer et al. 1998; Gerasimov et al. 2022). However, the intrinsic faintness of cool brown dwarfs largely limits their detection to the immediate Solar Neighborhood ( $d \lesssim 100$  pc).

\* Hubble Fellow

† Astronomy Department, Yale University, 52 Hillhouse Ave, New Haven, CT 06511, USA

The unprecedented sensitivity of JWST at near-infrared wavelengths where brown dwarfs are brightest enables detection of brown dwarfs deep into the Galactic halo (Ryan & Reid 2016; Aganze et al. 2022). Multiple brown dwarf candidates have already been identified in deep multi-band imaging surveys (Nonino et al. 2023; Glazebrook et al. 2023; Wang et al. 2023b; Hainline et al. 2023; Holwerda et al. 2023). However, confirmation and physical characterization of these distant brown dwarfs, including accurate measurement of temperatures, surface gravities, and compositions, requires spectroscopy.

The JWST Cycle 1 Treasury program Ultradeep NIRSpec and NIRCам Observations before the Epoch of Reionization (UNCOVER; Bezanson et al. 2022) aims to identify some of the highest redshift and faintest Epoch of Reionization (EoR) systems that are lensed by the massive  $z=0.308$  galaxy cluster Abell 2744. UNCOVER combines deep JWST NIRCам imaging over  $\sim 45$  arcmin<sup>2</sup> in seven filters (F115W, F150W, F200W, F277W, F356W, F410M, F444W) down to  $\sim 30$  AB mag (Weaver et al. 2023) with NIRSpec PRISM 0.6–5  $\mu$ m low-resolution spectroscopy. To date, UNCOVER has photometrically identified and characterized  $\sim 50,000$  galaxies in the Abell 2744 field, and has spectroscopically confirmed galaxies out to  $z \gtrsim 10$  (e.g., Wang et al. 2023a), characterized the hosts and supermassive black holes of multiple high-redshift active galactic nuclei (AGN; e.g., Goulding et al. 2023; Furtak et al. 2023), and performed the first spectroscopic analysis of low luminosity EoR galaxies (Atek et al. 2023).

In this article, we utilize the deep imaging and spectroscopy of UNCOVER to identify and spectroscopically characterize three T-type brown dwarfs. Section 2 summarizes the identification and observations of these sources. Section 3 describes our analysis of JWST/NIRSpec spectra, including classification, model fitting, and estimation of the distances by scaling model surface fluxes. Section 4 presents population simulations that justifies the detection of three T dwarfs in the narrow Abell 2744 field, and provides statistical constraints on the Galactic population membership. Section 5 summarizes our results. We note that these sources and analysis of the data presented here have also been reported contemporaneously by Langeroodi & Hjorth (2023).

## 2. IDENTIFICATION AND OBSERVATIONS

Catalog designations, coordinates, and AB magnitudes from Weaver et al. (2023) of the three sources presented here are listed in Table 1. Two of the sources were initially identified as candidate high-redshift AGN in UNCOVER NIRCам photometry (Labbe et al. 2023). The third source, 39243, was previously identified as the candidate T dwarf GLASS-BD-1 (aka “Nonino’s Dwarf”) based on multi-band NIRCам photometry from the Grism Lens-Amplified Survey from Space (GLASS) survey (Nonino et al. 2023; Glazebrook et al. 2023). All three sources were included in the first UNCOVER NIRSpec campaign.

NIRSpec/PRISM observations were obtained on 31 July – 2 August 2023 (UT), split over seven Multi-shutter array (MSA) masks. All observations were taken with a 2-POINT-WITH-NIRCam-SIZE2 dither pattern and a three shutter slitlet nod pattern at an angle of V3PA  $\sim 266^\circ$ . Sources 32265 and 33437 were observed on MSAs 3, 5, 6, and 7, using the NRSIRS2RAPID readout pattern for MSA 3 and NRSIRS2 for the rest, for a total of 14.3 hours. Source ID 39243 was observed on MSA 4 with readout pattern NRSIRS2 for a total of 4.4 hours. Full observational details will be presented in Price et al. (2023, in prep).

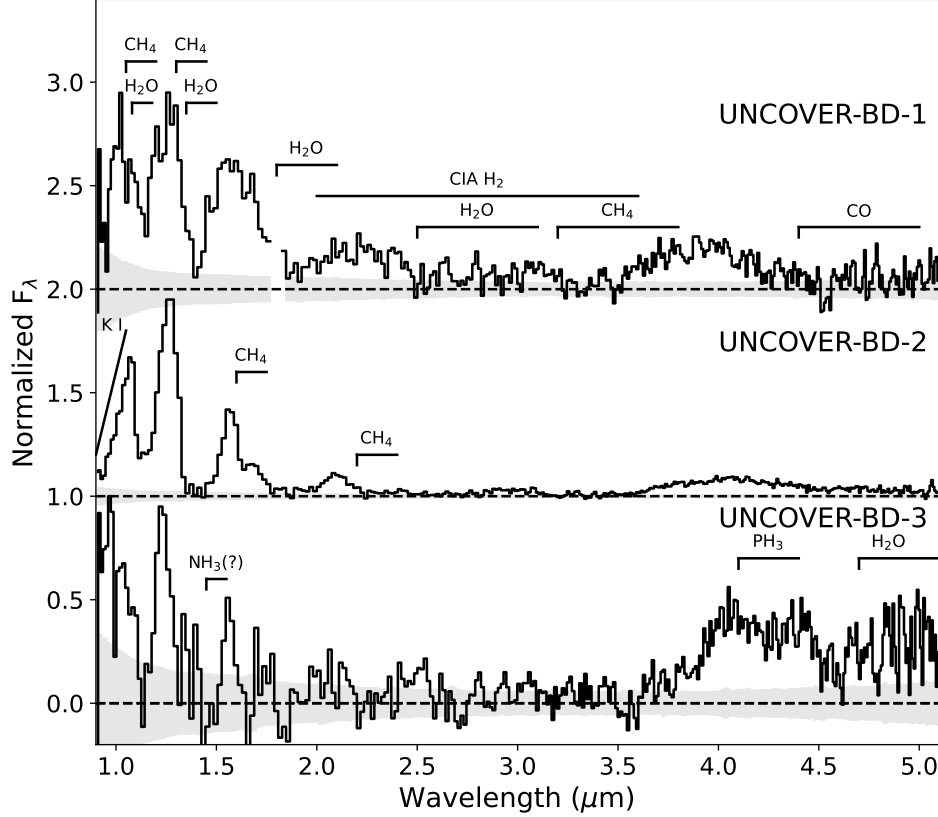
The spectra were reduced using `msaexp` (v0.6.10; [Brammer 2022](#)), starting from the level 2 data products downloaded from the Mikulski Archive for Space Telescopes (MAST)<sup>1</sup>, reduced using version 1.11.3 of the JWST Calibration pipeline ([Bushouse et al. 2023](#)). For each slit mask, `msaexp` corrects  $1/f$ -noise, finds and masks cosmic ray “snowballs,” and removes the bias in each individual frame. It then applies a world coordinate system, identifies each slit, and applies flat-fielding and photometric corrections. The 2D slits are combined and drizzled onto a common grid, a local background subtraction is applied, and spectra are then optimally extracted ([Horne 1986](#)). For the early spectroscopic reduction presented here (internal v0.3), flux calibration was modeled as a first-order polynomial determined by convolving the individual mask 1D spectra with the broad/medium band filters, and comparing to the total photometry ([Weaver et al. 2023](#)).

Figure 1 shows the calibrated JWST/NIRSpec spectra over the 1–5  $\mu\text{m}$  band. In the 1–2.5  $\mu\text{m}$  near-infrared region, we identify the 1.0, 1.25, 1.6, and 2.1  $\mu\text{m}$  flux peaks characteristic of cool brown dwarfs, shaped by strong  $\text{H}_2\text{O}$  and  $\text{CH}_4$  bands ([Burgasser et al. 2006b](#)). This is followed by a broad minimum spanning 2.3–3.5  $\mu\text{m}$  which encompasses  $\text{H}_2\text{O}$ ,  $\text{CH}_4$ , and collision-induced  $\text{H}_2$  absorption ([Leggett et al. 2015](#); [Linsky 1969](#)). A red peak emerges between 3.5 and 4.5  $\mu\text{m}$ , showing the most structure for Source 39243. This region is shaped by overlapping bands of  $\text{H}_2\text{O}$ ,  $\text{CH}_4$ ,  $\text{NH}_3$ ,  $\text{CO}_2$ ,  $\text{CO}$ , and possibly  $\text{PH}_3$  in cool brown dwarfs ([Yamamura et al. 2010](#); [Sorahana & Yamamura 2012](#); [Leggett et al. 2015](#); [Miles et al. 2020](#); [Beiler et al. 2023](#)), as discussed further below. We conclude from these spectral morphologies that all three sources are low-temperature brown dwarfs, and are hereafter designated as UNCOVER-BD sources.

### 3. SPECTRAL ANALYSIS

We classified the sources by comparing their 1–2.4  $\mu\text{m}$  spectra to L and T dwarf spectral standards from the SpeX Prism Library Analysis Toolkit (SPLAT; [Burgasser & Splat Development Team 2017](#)). We identified the standard with the smallest

<sup>1</sup> 10.17909/8k5c-xr27



**Figure 1.** JWST/NIRSpec PRISM spectra of the three brown dwarf candidates observed by UNCOVER in  $F_\lambda$  units (black lines with grey shaded uncertainties), normalized in the 1.1–1.3  $\mu\text{m}$  region to a maximum value of 0.95. Each spectrum is offset by a constant (dashed lines), and major spectral features in the 1–5  $\mu\text{m}$  region are labeled. A bad pixel at 1.8  $\mu\text{m}$  has been masked out in the spectrum of UNCOVER-BD-1.

reduced  $\chi_r^2$  residual,<sup>2</sup> shown in the left panels of Figure 2. For UNCOVER-BD-1, the T1 standard provides the best overall fit, but has clear deviations in each of the  $J$ -,  $H$ -, and  $K$ -band spectral peaks. In particular, UNCOVER-BD-1 shows excess flux on the blue side of the  $H$ -band while having a relatively suppressed  $K$ -band. As discussed below, we infer these deviations are caused by subsolar metallicity. UNCOVER-BD-2 is an excellent match to the T6 standard, while UNCOVER-BD-3 equally matches T8 and T9 standards, likely due to the spectrum’s lower signal-to-noise.

To quantify the physical properties of these sources, we compared the JWST/NIRSpec spectra to five sets of low-temperature atmosphere models: BT-Settl (Allard et al. 2012), ATMO (Phillips et al. 2020), Sonora-Bobcat (Marley et al. 2021), Sonora-Cholla (Karlidi et al. 2021), and LOWZ (Meisner et al. 2021). These models span the temperature range of T- and Y-type dwarfs (roughly 500–1500 K), with varying parameters and treatments for metal composition, opacities, chemical equi-

<sup>2</sup> We compute chi-square as  $\chi^2 \equiv \sum_i \frac{(O_i - \alpha C_i)^2}{\sigma_i^2}$ , where  $\mathbf{O}$  is the observed spectrum,  $\mathbf{C}$  the comparison template,  $\sigma$  the observed spectrum uncertainties, and  $\alpha = \frac{\sum_i O_i C_i / \sigma_i^2}{\sum_i C_i^2 / \sigma_i^2}$  is a scaling factor that minimizes  $\chi^2$ . We compute reduced chi-square as  $\chi_r^2 \equiv \chi^2 / (N - 1)$ , where  $N$  is the number of spectral data points.

**Table 1.** Properties of the UNCOVER T Dwarfs

Property	UNCOVER-BD-1	UNCOVER-BD-2	UNCOVER-BD-3 <sup>a</sup>	Ref
HST & JWST Astrometry & Photometry <sup>b</sup>				
Coordinate	J00140901-3022126	J00141114-3021585	J00140333-3021217	[1]
MSA ID <sup>c</sup>	32265	33437	39243	[1]
F814W (AB)	27.38±0.31	...	...	[1]
F115W (AB)	28.26±0.11	27.34±0.06	28.00±0.06	[1]
F125W (AB)	...	...	27.57±0.49	[1]
F150W (AB)	28.06±0.09	28.10±0.10	28.81±0.18	[1]
F160W (AB)	...	...	27.49±0.69	[1]
F200W (AB)	28.04±0.10	28.87±0.19	29.71±0.35	[1]
F277W (AB)	28.25±0.08	29.03±0.16	29.16±0.14	[1]
F356W (AB)	27.57±0.03	28.06±0.06	27.69±0.03	[1]
F410M (AB)	27.04±0.04	26.71±0.03	...	[1]
F444W (AB)	27.28±0.04	26.97±0.03	25.637±0.005	[1]
Spectral Properties				
Integration Time (hr)	14.3	14.3	4.4	[2]
Spectral Type	sdT1	T6	T8–T9	[2]
$T_{eff}^d$ (K)	1300 (1100–1500)	1000 (1000–1100)	550 (500–700)	[2]
$\log g^d$ (cgs)	5.0 (4.5–5.0)	5.25 (5.25–5.5)	5.25 (5.0–5.5)	[2]
$[M/H]^d$	-1.0	0.0	-0.5	[2]
Other Inferred Properties				
$d_{model}^e$ (kpc)	4.5±1.2	2.32±0.23	0.87±0.30	[2]
$\mathcal{P}$ (thin disk)	<1%	16%	75%	[2]
$\mathcal{P}$ (thick disk)	76%	79%	25%	[2]
$\mathcal{P}$ (halo)	24%	6%	<1%	[2]

<sup>a</sup> aka GLASS-BD-1 or "Nonino's Dwarf" (Nonino et al. 2023).

<sup>b</sup> Photometry in AB magnitudes from Weaver et al. (2023) (internal version 3.0.0).

<sup>c</sup> Multi-Slit Array identification number (Weaver et al. 2023, internal version 2.2.1).

<sup>d</sup> Single values based on best fits to LOWZ models, while ranges for  $T_{eff}$  and  $\log g$  encapsulate the fits to all five models examined.

<sup>e</sup> Based on scaling surface fluxes of best model fits to observed apparent spectral fluxes and assuming a radius of 1 Jupiter radius.

**References**— [1] Weaver et al. (2023); [2] This paper.

librium, and cloud formation. We focused on models with surface gravities  $\log g \geq 4$  (cgs), consistent with ages  $\gtrsim 100$  Myr. We smoothed and interpolated each model to match the resolution of the NIRSpec/PRISM data over the 1–5  $\mu\text{m}$  band, scaling model fluxes to minimize  $\chi_r^2$  residuals. We performed a simple grid fit, identifying the lowest  $\chi_r^2$  match to the data within each grid.

Of the five model sets, the LOWZ models consistently provided the best fits (Figure 2), although all five models gave equivalent values for temperature and surface gravity. The LOWZ models are also computed at subsolar metallicities, and it is notable that both UNCOVER-BD-1 and UNCOVER-BD-3 are best fit to subsolar metallicity models. Our inferred temperature for UNCOVER-BD-3,  $500 \text{ K} \lesssim T_{eff} \lesssim 700 \text{ K}$ , is also consistent with the 650 K estimate by Nonino et al. (2023) based on NIRCам photometry. Finally, we note that CO, CH<sub>4</sub>, and NH<sub>3</sub> abundances are strongly affected by non-equilibrium mixing in brown dwarf atmospheres, and all three



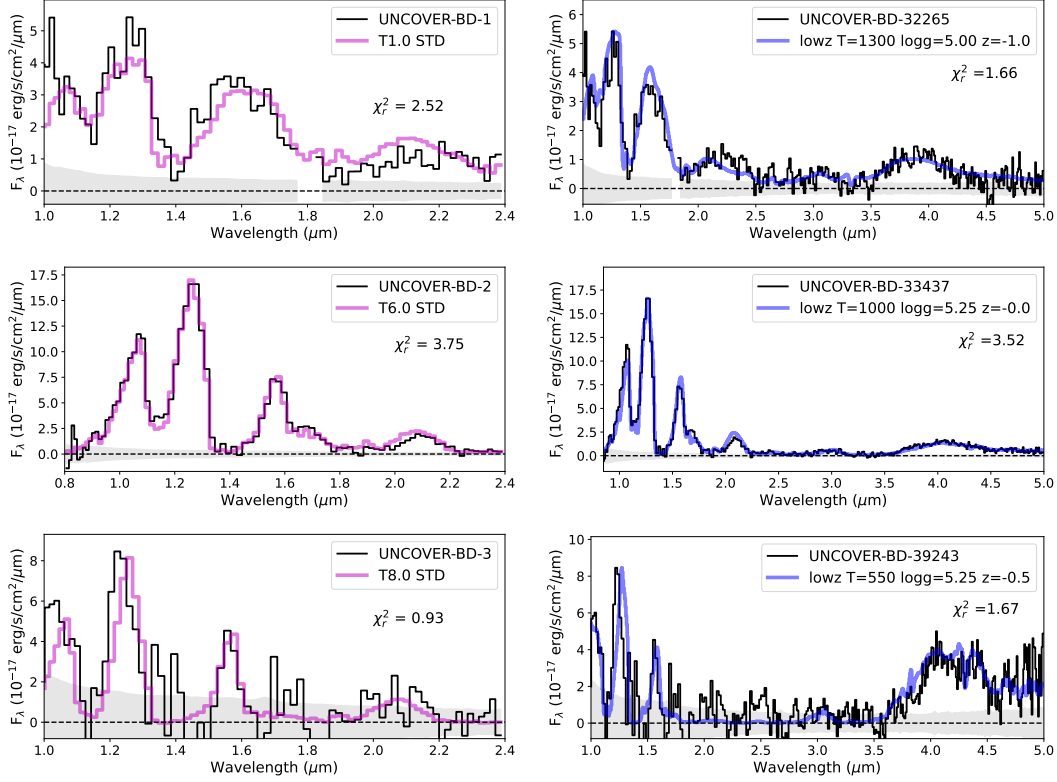


**Figure 2.** (Left panels): Comparison of the 1-2.4  $\mu\text{m}$  JWST/NIRSpec PRISM spectra (black lines with grey shaded uncertainties in apparent flux density units) to their best-fit near-infrared spectral standards from SPLAT (magenta lines). Standard spectra are from [Burgasser et al. \(2004, 2006a\)](#). (Right panels): Best-fits LOWZ models to the full 1-5  $\mu\text{m}$  spectra (blue lines), with parameters indicated in the legends.

molecules exhibit absorption features in the 1-5  $\mu\text{m}$  range (Figure 1). The best-fit ATMOS and Sonora-Cholla models both indicate enhanced vertical mixing with  $\log \kappa_{zz} = 7-8$  (cgs) for UNCOVER-BD-1, while UNCOVER-BD-2 and UNCOVER-BD-3 are best matched to low  $\kappa_{zz}$ /chemical equilibrium models.

The atmosphere models are computed as surface fluxes; hence, our fits to apparent flux densities constraint the scale factor  $\alpha = (R/d)^2$ , where  $R$  is the radius of the source and  $d$  its distance. Assuming a common radius of 1 Jupiter radius for all three brown dwarfs, averaging over all best-fit models, and ignoring the presence of binary companions, we infer the spectroscopic distance estimates listed in Table 1. Our distance estimate of  $870 \pm 300$  pc for UNCOVER-BD-3 overlaps with the 570-720 pc estimate by [Nonino et al. \(2023\)](#), while the other two brown dwarfs have estimated distances exceeding 2 kpc. To our knowledge, these are the most distant T dwarfs to have measured spectroscopy.

#### 4. POPULATION CONSTRAINTS

As the Abell 2744 field is at a high Galactic latitude ( $b = -81^\circ$ ), the kpc-scale distances of these brown dwarfs translate into large vertical offsets from the Galactic plane, and hence a high likelihood of being members of the thick disk or halo popu-

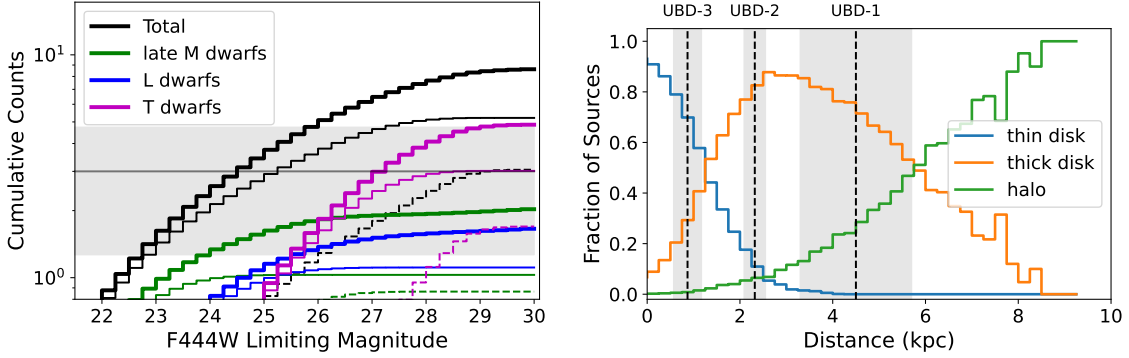


**Figure 3.** (Left) Cumulative number counts of expected L and T dwarfs in the UNCOVER field of view as a function of limiting F444W magnitude. Sources are required to be detected ( $<30$  AB mag) in at least three filters. Counts are broken down by spectral class (L dwarfs in blue, T dwarfs in magenta, total in black) and by population (thin disk as solid lines, thick disk as dashed lines, halo as dotted lines, total as thick solid lines). The grey horizontal line and band delineates the number of confirmed T dwarfs in the Abell 2744 field with Poisson uncertainties. (Right): Relative fraction of thin disk (blue line), thick disk (orange line), and halo (green line) as a function of distance for the T dwarfs in our simulation. The vertical regions indicate the estimated distances and  $1\sigma$  uncertainties of the three T dwarfs reported here.

lations. To assess population membership and to ascertain whether the number of T dwarfs found is consistent with expectations, we constructed a Galactic population simulation of thin disk, thick disk, and halo low-mass stars and brown dwarfs, accounting for substellar evolution and population spatial distributions. Full details of the simulation are provided in the Appendix.

Figure 3 shows the overall predicted numbers of detectable ultracool dwarfs in the Abell 2744 field based on these simulations, with the numbers of late-M, L, and T dwarfs disaggregated. At magnitudes  $F444W \gtrsim 26$  AB, T dwarfs are the dominant population of ultracool dwarfs in this field, and are primarily thin disk sources. By  $F444W = 30$  AB, our simulations predict approximately 5 T dwarfs in the Abell 2744 field,  $\approx 60\%$  from the thin disk,  $\approx 35\%$  from the thick disk, and  $\lesssim 5\%$  from the halo. The detection of 3 T dwarfs in the limited spectroscopic follow-up of targets thus far, and perhaps 1-2 strong candidates in photometric data (Greene et al. 2023), is fully consistent with these simulations. Only  $\sim 2$  M dwarfs and  $\sim 1$ – $2$  L dwarfs are expected in the Abell 2744 field, in 1:1 and 2:1 ratios of thin:thick disk members; and a negligible number of Y dwarfs due to their intrinsic faintness. There are also few ( $\sim 0$ – $1$ ) halo ultracool dwarfs expected in this field despite its depth, although this prediction is more sensitive to the poorly-constrained atmospheric and evolutionary properties of metal-poor brown dwarfs. Hence, while the brown dwarf sample in the narrow Abell 2744 field may be small, it is a mixture of different Galactic populations that is distinct from the local Solar Neighborhood.

Our simulations allow us to assess the individual population memberships of the three UNCOVER T dwarfs based on their estimated distances. Figure 3 shows how



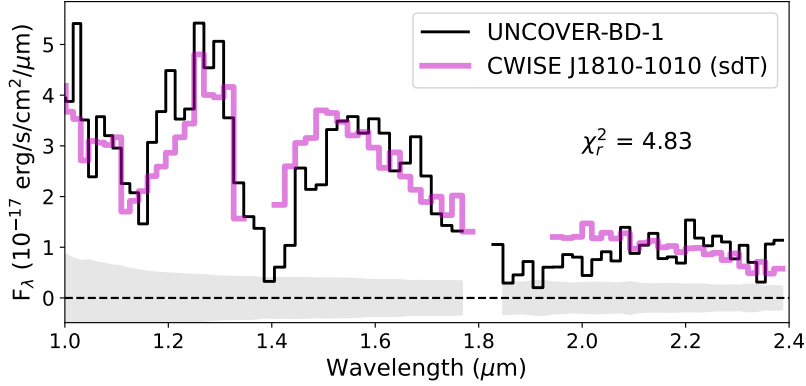


**Figure 4.** Comparison of the spectra of UNCOVER-BD-1 (black line) and the extreme T subdwarf CWISE J1810-1010 (magenta line; data from [Schneider et al. 2020](#)). The latter is scaled to minimize the  $\chi_r^2$  residuals between the data. Note that breaks in the CWISE J1810-1010 spectrum represent regions of strong telluric absorption in ground-based spectroscopy.

the relative fractions of thin disk, thick disk, and halo T dwarfs varies as a function of distance along the Abell 2744 line of sight. Beyond 1.4 kpc, thick disk T dwarfs start to outnumber thin disk T dwarfs; beyond 6 kpc, halo T dwarfs start to outnumber thick disk T dwarfs. The estimated distances of the UNCOVER-BDs span these thresholds, with UNCOVER-BD-1 in particular having 76% and 24% probabilities of being a thick disk or halo member, respectively. Our small spectral sample is therefore representative of brown dwarfs in the Milky Way’s three main populations.

## 5. DISCUSSION OF INDIVIDUAL SOURCES

### 5.1. *The Distant T subdwarf UNCOVER-BD-1*

The subsolar metallicity features in the spectrum of UNCOVER-BD-1 are fully consistent with this source’s probable association with the thick disk or halo. The atmosphere parameters inferred for this source closely match those of CWISE J1810-1010, a nearby T subdwarf identified in the citizen science Backyard Worlds: Planet 9 program ([Schneider et al. 2020](#); [Kuchner et al. 2017](#)). We compare the spectrum of these two sources in Figure 4. The T subdwarf more accurately reproduces the widened 1.1  $\mu\text{m}$  absorption feature and relatively featureless *H*-band peak characteristic of metal-poor brown dwarfs, but shows excess flux on the blue wings of the *H*- and *K*-band peaks. Of course, it is unlikely given the few T subdwarfs currently known that a perfect match would have occurred ([Zhang et al. 2019a](#); [Meisner et al. 2021](#)). Nevertheless, the similarities combined with both model fitting and population analysis supports the interpretation of this source as a metal-poor brown dwarf. We note that parallax measurement of CWISE J1810-1010 by [Lodieu et al. \(2022\)](#) has shown this source to be considerably cooler ( $\sim 800$  K) and closer (9 pc) than initial estimates, and the same may be true of our estimates of UNCOVER-BD-1.

### 5.2. *Phosphine in the Spectrum of UNCOVER-BD-3?*

Our coldest source, UNCOVER-BD-3/GLASS-BD-1/Nonino’s Dwarf is notable for the significant structure present in its 4–4.5  $\mu\text{m}$  peak (Figure 5). This region is shaped by multiple molecular species, including  $\text{H}_2\text{O}$ ,  $\text{CH}_4$ ,  $\text{NH}_3$ ,  $\text{CO}_2$ ,  $\text{CO}$ ,  $\text{PH}_3$ , and  $\text{H}_2\text{S}$ , with relative abundances influenced by non-equilibrium chemistry and metallicity, (Griffith & Yelle 1999; Noll et al. 2000; Saumon et al. 2006; Visscher et al. 2006; Yamamura et al. 2010; Leggett et al. 2015; Miles et al. 2020; Beiler et al. 2023). We compare the spectrum of UNCOVER-BD-3 in this region to the JWST/NIRSpec spectrum of the  $T_{\text{eff}} \approx 450$  K Y0 dwarf WISE J035934.06-540154.6 (hereafter W0359-54; Kirkpatrick et al. 2012; Leggett et al. 2016; Beiler et al. 2023). Both sources show absorption from the red wing of the 3.3  $\mu\text{m}$   $\text{CH}_4$   $\nu_3$  band, the 4.5  $\mu\text{m}$  bandhead of  $\text{CO}$  (enhanced by mixing), and  $\text{H}_2\text{O}$  extending toward and beyond 5  $\mu\text{m}$ . However, while W0359-54 shows a distinct minimum over 4.2–4.4  $\mu\text{m}$ , a feature that has been associated with  $\text{CO}_2$  absorption (Yamamura et al. 2010; Sorahana & Yamamura 2012; Beiler et al. 2023), this depression is broader and lacks the sharp  $\text{CO}_2$  bandhead in the spectrum of UNCOVER-BD-3.

We investigated this distinction by comparing absorption coefficients  $\alpha_i = n_i \sigma_i$  for the seven species  $i$  listed above, using cross-sections  $\sigma_i$  at  $T = 600$  K provided by the EXOMOL cross-section server<sup>3</sup> (Hill et al. 2013; Tennyson & Yurchenko 2012). Relative abundances  $n_i/n$  at  $T = 600$  K and  $P = 10$  bar ( $n = 1.2 \times 10^{20} \text{ cm}^{-3}$ ) are based on non-equilibrium chemistry for  $\text{H}_2\text{O}$ ,  $\text{CH}_4$ ,  $\text{CO}$ ,  $\text{NH}_3$  and  $\text{PH}_3$  (Saumon et al. 2006; Visscher et al. 2006), and equilibrium chemistry for  $\text{H}_2\text{S}$  (Visscher et al. 2006). For  $\text{CO}_2$ , we adopted the conjecture of Yamamura et al. (2010) that  $N_{\text{CO}_2}/N_{\text{CO}} \approx 10^{-3}$ , and thus exceeds equilibrium abundances by several orders of magnitude (Lodders & Fegley 2002). Yamamura et al. (2010) notes that this  $\text{CO}_2$  enrichment even exceeds expectations for disequilibrium mixing abundances, but is necessary to explain the distinct bandhead seen in solar-metallicity T and Y dwarf spectra at 3–5  $\mu\text{m}$ . The mechanism for this enrichment has yet to be determined. Indeed, Figure 5 shows that even with these assumptions, it is  $\text{PH}_3$ , not  $\text{CO}_2$  that should be the primary absorber around 4.2  $\mu\text{m}$ . Introducing into this analysis reduced metal abundances in the atmosphere of UNCOVER-BD-3, suggested by our model fits and modest probability of thick-disk membership (25%), would further reduce the abundance of  $\text{CO}_2$  relative to single-metal species such as  $\text{H}_2\text{O}$  or  $\text{PH}_3$ , just as  $\text{TiO}$  is reduced relative to  $\text{CaH}$  in the optical spectra of M-type subdwarfs (Mould & McElroy 1978; Gizis 1997). While the blue wing of the 4.2  $\mu\text{m}$  feature in UNCOVER-BD-3 could be caused by a relative strengthening of  $\text{H}_2\text{O}$  over  $\text{CH}_4$ , we would expect to see more absorption in the 4.8–5.0  $\mu\text{m}$  region as well, but instead see a slight rise in flux. Neither  $\text{NH}_3$  nor  $\text{H}_2\text{S}$  show opacity trends that could explain the structure of this feature.

<sup>3</sup> See <https://www.exomol.com/data/data-types/xsec>. Cross-sections are based on molecular line lists from Hill et al. (2013); Li et al. (2015); Yurchenko et al. (2011); Polyansky et al. (2018); Azzam et al. (2016); Sousa-Silva et al. (2015) and Yurchenko et al. (2020).

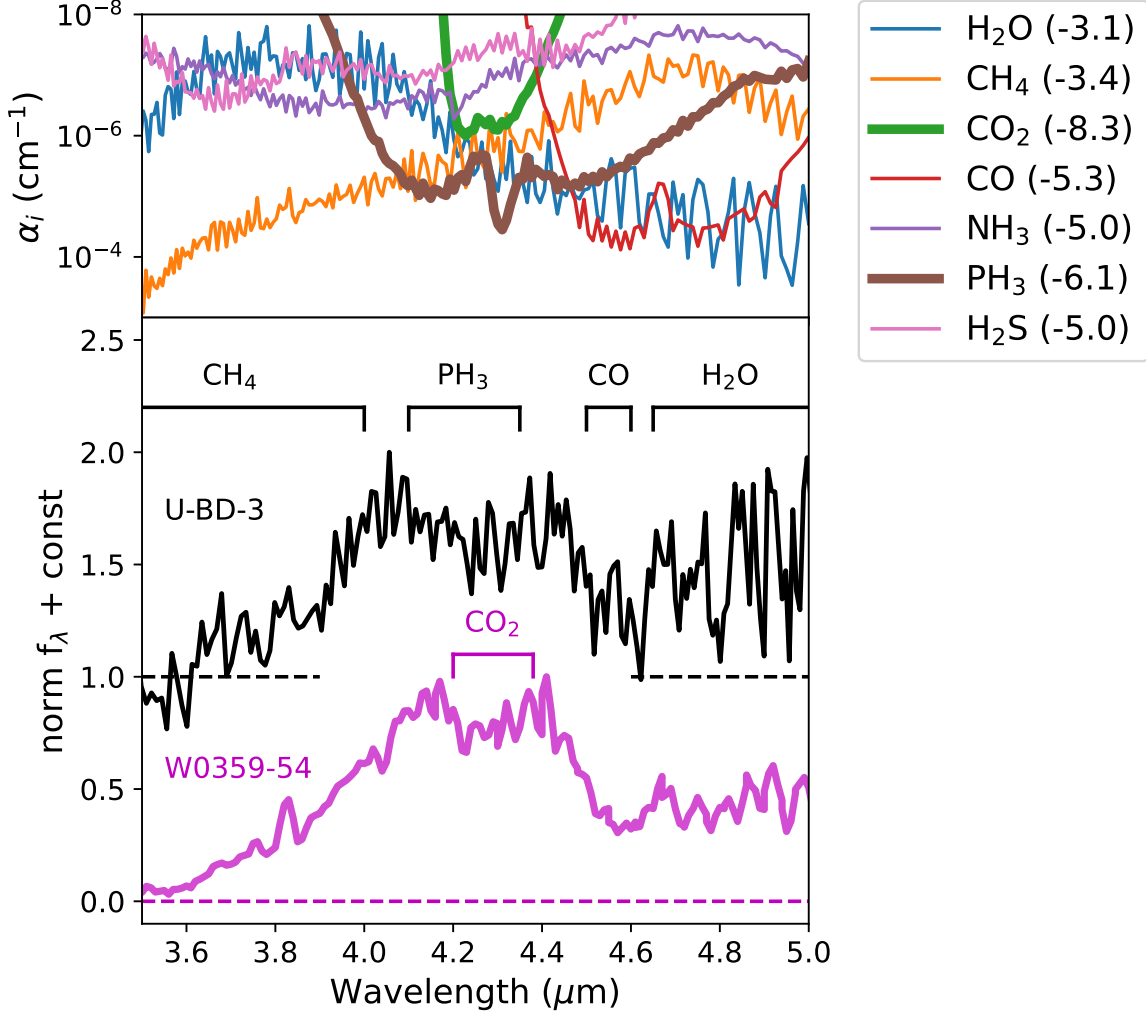


**Figure 5.** (Top panel) Absorption coefficients for  $\text{H}_2\text{O}$ ,  $\text{CH}_4$ ,  $\text{NH}_3$ ,  $\text{CO}_2$ ,  $\text{CO}$ ,  $\text{PH}_3$ , and  $\text{H}_2\text{S}$  in the 3.5–5  $\mu\text{m}$  region based on EXOMOL cross-sections (Hill et al. 2013; Tennyson & Yurchenko 2012) and relative abundances based on equilibrium and non-equilibrium chemistry (log values of relative abundance for each species are listed in the legend; see text for details). The strongest absorber at a given wavelength is toward the bottom of this plot. Absorption coefficients for  $\text{CO}_2$  (in green) and  $\text{PH}_3$  (in brown) are highlighted. (Bottom panel) Normalized spectra of UNCOVER-BD-3 (black line) and the Y0 dwarf W0359-54 (magenta line) in the 3.5–5  $\mu\text{m}$  region, with the former offset for comparison (dashed lines). We identify the dominant absorbing species across this band based on the top panel, including  $\text{PH}_3$  for UNCOVER-BD-3 and  $\text{CO}_2$  for W0359-54.

We therefore claim that the 4.2  $\mu\text{m}$  feature in UNCOVER-BD-3 is  $\text{PH}_3$ , not  $\text{CO}_2$ , and its presence may serve as an indicator of subsolar metallicity among the coldest brown dwarfs. The presence of multiple overlapping molecular species in this region, whose abundances are sensitive to mixing and metallicity, highlights its importance in atmospheric chemical studies of cold brown dwarfs and warm exoplanets (Miles et al. 2023).

## 6. SUMMARY

We report JWST/NIRSpec spectroscopy of three distant T dwarfs identified in the Abell 2744 lensing field by the UNCOVER JWST Legacy Survey. All three objects display the characteristic signatures of low temperature brown dwarf atmospheres, and are all well-matched in the 1–2.5  $\mu\text{m}$  region to T1, T6, and T8–T9 standards. Spectral model fits confirm these identifications, and further indicate that UNCOVER-BD-1 and perhaps UNCOVER-BD-3 are metal-poor. These fits provide robust estimates of the distances of these sources that place them between 0.9–4.5 kpc, making them the most distant T dwarfs with confirming spectroscopy to date. UNCOVER-BD-1 and UNCOVER-BD-2 in particular are sufficiently distant to have a high probability of membership in the thick disk. Similarities in the spectra of UNCOVER-BD-1 and the T subdwarf CWISE J1810-1010 supports the metal-poor nature of both sources. For UNCOVER-BD-3, the structure of the 4.2  $\mu\text{m}$  peak indicates the signature of  $\text{PH}_3$  absorption rather than  $\text{CO}_2$  as seen in other T and Y dwarfs, and may reflect metallicity effects on molecular chemistry in cold brown dwarf atmospheres. Our population simulations indicate that the Abell 2744 field should contain roughly 1–2 L-type and 5 T-type brown dwarfs, with one-third of these being members of the Galactic thick disk. While modest, this reflects the yield from a very small field of view (only seven NIRSpec pointings in this study), and further investigations of an assemble of deep JWST pointings will uncover a larger and statistically useful sample for characterizing the oldest, metal-poor brown dwarfs in the Milky Way (Nonino et al. 2023; Hainline et al. 2023; Holwerda et al. 2023).

We dedicate this paper to the memory of Dr. Mario Nonino, discoverer of the first brown dwarf discovery made with JWST, GLASS-BD-1/UNCOVER-BD-3/Nonino’s Dwarf, who passed way suddenly during the completion of this paper. Dr. Nonino will be remembered as a friendly and collaborative colleague. This work is based in part on observations made with the NASA/ESA *Hubble Space Telescope* (HST) and the NASA/ESA/CSA *James Webb Space Telescope* (JWST). Some of the data presented in this paper were obtained from the Mikulski Archive for Space Telescopes at the Space Telescope Science Institute. The specific observations analyzed can be accessed via [10.17909/8k5c-xr27](https://archive.stsci.edu/10.17909/8k5c-xr27). These observations are associated with JWST programs JWST-GO-2561, JWST-ERS-1324, and JWST-DD-2756; and with HST programs HST-GO-11689, HST-GO-13386, HST-GO/DD-13495, HST-GO-13389, HST-GO-15117, and HST-GO/DD-17231. Support for program JWST-GO-2561 was provided by NASA through a grant from the Space Telescope Science Institute, which is operated by the Associations of Universities for Research in Astronomy, Incorporated, under NASA contract NAS 5-03127. A.J.B. and R.G. acknowledge support from JWST program GO-2559 and NASA/ADAP grant 21-ADAP21-0187. J.E.G. and A.D.G. acknowledge support from NSF/AAG grant # 1007094. J.E.G. also acknowledges support from NSF/AAG grant # 1007052. A.Z. acknowledges support by Grant No. 2020750 from the United States-Israel Binational Science Foundation (BSF) and Grant No. 2109066 from the United States National Science Foundation (NSF), and by the Ministry of Science & Technology of Israel. The Cosmic Dawn Center is funded by the Danish National Research Foundation (DNRF) under grant #140. This work has received funding from the Swiss State Secretariat for Education, Research and Innovation (SERI) under contract number MB22.00072, as well as from the Swiss National Science Foundation (SNSF) through project grant 200020 207349. R.B. acknowledges support from the Research Corporation for Scientific Advancement (RCSA) Cottrell Scholar Award ID No: 27587 and from the National Science Foundation NSF-CAREER grant # 2144314. P.D. acknowledges support from the Dutch Research Council (NWO) through the award of the VIDI Grant 016.VIDI.189.162 (“ODIN”) and the European Commission’s and University of Groningen’s CO-FUND Rosalind Franklin program. R.P.N. acknowledges funding from JWST programs GO-1933 and GO-2279. Support for this work was provided by NASA through the NASA Hubble Fellowship grant HST-HF2-51515.001-A awarded by the Space Telescope Science Institute, which is operated by the Association of Universities for Research in Astronomy, Incorporated, under NASA contract NAS5-26555. The research of C.C.W. is supported by NOIRLab, which is managed by the Association of Universities for Research in Astronomy (AURA) under a cooperative agreement with the National Science Foundation. R.P. and D.M. acknowledge support from JWST program GO-2561.

*Facilities:* JWST(NIRCam), JWST(NIRSpec), HST(ACS), HST(WFC3)

*Software:* *astropy* (Astropy Collaboration et al. 2013, 2018, 2022), *msaexp* (Brammer 2022), JWST Calibration pipeline (Bushouse et al. 2023), SPLAT (Burgasser & Splat Development Team 2017),

## APPENDIX

### A. ULTRACOOOL DWARF GALACTIC POPULATION SIMULATIONS

Here we describe in detail the ultracool dwarf population simulations discussed in Section 4. These simulations are based on Monte Carlo approaches previously presented in Burgasser (2004, 2007); Bardalez Gagliuffi et al. (2019); Hsu et al. (2021); and Aganze et al. (2022), with additional modifications described here to account for the spatial and spectral properties of ultracool dwarfs in different Galactic populations. See Reid et al. (1999); Day-Jones et al. (2013); Burningham et al. (2013); Ryan & Reid (2016); van Vledder et al. (2016); Best et al. (2020); Kirkpatrick et al. (2021); and Ryan et al. (2022) for other approaches.

We modeled our ultracool dwarf sample as three populations representing the thin disk, the thick disk, and the halo, the latter treated as a single population (cf. Carollo et al. 2008). We generated a set of  $5 \times 10^5$  masses between 0.01–0.1  $M_{\odot}$  distributed as a power-law mass function with  $dN/dM \propto M^{-0.6}$  (Kirkpatrick et al. 2021) that were common to the three populations; and three uniform distributions of ages, one spanning 0.5–8 Gyr for the thin disk, and two spanning 8–10 Gyr for the thick disk and halo. These samples were then evolved to present-day temperatures ( $T_{eff}$ ), surface gravities ( $\log g$ ), and luminosities using the Sonora-Bobcat models (Marley et al. 2021), applying the  $[M/H] = 0$  models for the thin disk and  $[M/H] = -0.5$  models for the thick disk and halo.<sup>4</sup>

These physical parameters were mapped to observational parameters of spectral type and absolute magnitude using a combination of empirical relations and theoretical atmosphere models. The empirical relations are based on a sample of local, largely solar-metallicity ultracool dwarfs, and are most appropriate for thin disk objects; see Zhang et al. (2019b) and Gonzales et al. (2021) for relations appropriate for metal-poor M- and L-type ultracool dwarfs. Temperatures were first mapped to spectral types from M6 to Y2 using an updated calibration from<sup>5</sup> Pecaut & Mamajek (2013). We then constructed spectral type/absolute magnitude relations for six wide-field JWST/NIRCam filters, F115W, F150W, F200W, F277W, F356W, and F444W, anchoring to existing spectral type/absolute magnitude relations in proximate filters. For spectral types M6 to T7, we used the spectral type/absolute magnitude relations of Dupuy & Liu (2012) for filters MKO J, MKO H, MKO K, MKO  $L_P$ , IRAC [3.6], and IRAC [4.5]. For spectral types T8 to Y2, we used the spectral type/absolute

<sup>4</sup> A comprehensive set of lower metallicity evolutionary models for cold brown dwarfs using up-to-date opacities are not yet publicly available; see Gerasimov et al. (2020).

<sup>5</sup> E. Mamajek 2022; see [https://www.pas.rochester.edu/~emamajek/EEM\\_dwarf\\_UBVIJHK\\_colors\\_Teff.txt](https://www.pas.rochester.edu/~emamajek/EEM_dwarf_UBVIJHK_colors_Teff.txt).



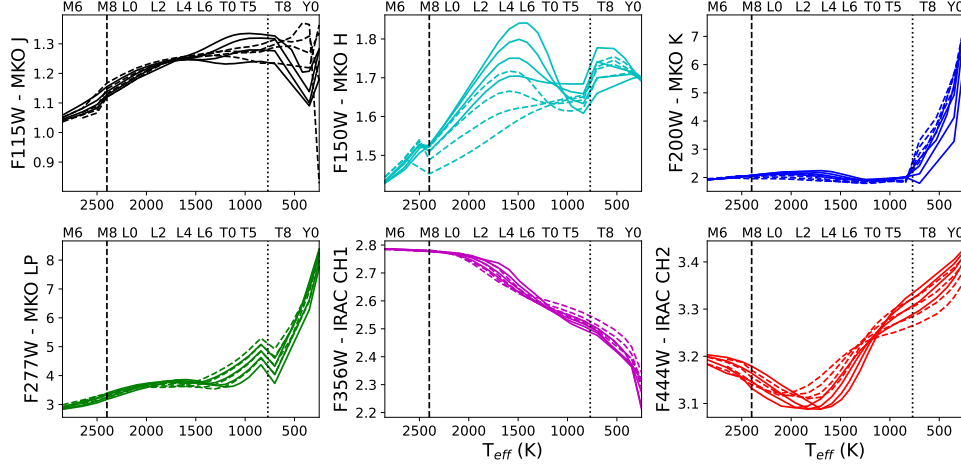


**Figure 6.** Filter color correction terms between JWST/NIRCam filters and reference filters used for empirical relations as a function of  $T_{\text{eff}}$ . Corrections for a variety of surface gravities and for solar-scaled metallicities  $[M/H] = 0$  and  $-0.5$  are shown by the various lines. Note that the models used to compute these corrections changes from BT-Settl (Allard et al. 2012) to Sonora-Bobcat (Marley et al. 2021) at  $T_{\text{eff}} = 2400$  K, and the reference filters and absolute magnitude relations used change at spectral type T8 ( $T_{\text{eff}} = 700$  K; see Table 2).

magnitude relations of Kirkpatrick et al. (2021) for filters MKO J, 2MASS H, IRAC [3.6], and IRAC [4.5]. Color terms between these filters and JWST/NIRCam filters were computed using atmosphere models of the appropriate temperature and metallicity, and for surface gravities  $4.0 \leq \log g \leq 5.5$  (in  $\text{cm/s}^2$ ). For  $T_{\text{eff}} > 2400$  K, we used the BT-Settl models (Allard et al. 2012); for  $T_{\text{eff}} \leq 2400$  K we used the Sonora-Bobcat models (Marley et al. 2021). Figure 6 displays the color terms between the empirical and JWST/NIRCam filters, and Figure 7 displays the resulting JWST/NIRCam absolute magnitude/spectral type relations, tabulated in Table 2. Uncertainties on these values vary as a function of spectral type, and a conservative estimate of 0.5 mag is appropriate for most of the spectral type range shown. Comparable relations for a broader set of JWST/NIRCam filters can be found in Sanghi et al. (2023).

Distances for each source were assigned by drawing from projected stellar density distributions along the Abell 2744 line of sight using the Milky Way structure parameters of Jurić et al. (2008). The maximum distances for these distributions were set by the absolute F444W magnitude of each source and an assumed limiting magnitude of 30 AB. For the M dwarfs in the simulation, maximum distances can exceed 30 kpc; for the T dwarfs, maximum distances range over 3–10 kpc. We ignored both unresolved multiplicity and statistical scatter for these limits, factors that were considered insignificant given the small size of our search area and final sample. Each source was assigned a distance according to the line-of-sight density distribution for its population truncated at this maximum distance, and then assigned a corresponding apparent magnitude.

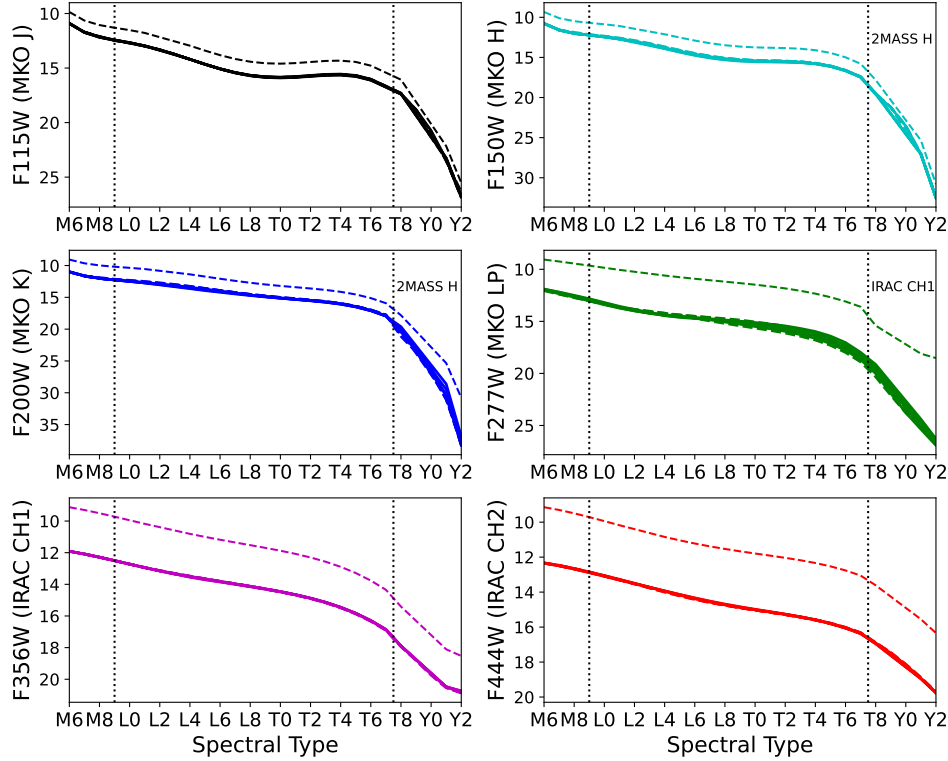


**Figure 7.** Absolute magnitudes in six JWST/NIRCам filters as a function of spectral type adopted in this study. The solid lines delineate the absolute magnitudes in the NIRCам filters in AB magnitudes, while the dashed lines indicate the original absolute magnitudes in the matched reference filter (indicated in the y-axis label and Table 2). Note that the reference filter and empirical relation used changes at spectral type T7/T8. The increasing divergence between reference filter and NIRCам filter relations toward longer wavelengths largely reflects the divergence between the Vega and AB magnitude systems.

To construct a composite population, we randomly drew sources with replacement from our thin disk, thick disk, and halo samples, ensuring that the relative numbers of sources within 500 pc matched the local fractions in the [Jurić et al. \(2008\)](#) model: thick disk/thin disk = 12% and halo/thin disk = 0.5%. We further required that apparent magnitudes in at least three NIRCам filters were brighter than the 30 AB limit to ensure multi-band detection. Finally, we computed a scaling factor<sup>6</sup> to correct the cumulative number of L1–T8 dwarfs within  $d = 100$  pc in our simulation to the expected number of these sources in the same volume based on the measured local space density  $\rho_{obs} = (1.09 \pm 0.06) \times 10^{-3} \text{ pc}^{-3}$  ([Kirkpatrick et al. 2021](#)) and the imaged area of  $\Omega = 45 \text{ arcmin}^2$ .

<sup>6</sup> The scaling factor  $\frac{N_{true}}{N_{sim}} = \frac{\rho_{obs}}{N_{sim}(<d)} \frac{\Omega}{3} d^3$  assumes a uniform spatial volume within our scaling distance  $d = 100$  pc; see [Kirkpatrick et al. \(2019\)](#) and [Best et al. \(2020\)](#) for discussion on the spatial isotropy of ultracool dwarfs within 20 pc of the Sun.

**Table 2.** JWST/NIRCam Absolute Magnitude Relations

SpT	$T_{eff}$ (K) <sup>a</sup>	[M/H]	Model	F115W	F150W	F200W	F277W	F356W	F444W
	Base magnitude	M6-T7 <sup>b</sup>		MKO J	MKO H	MKO K	MKO $L_P$	IRAC [3.6]	IRAC [4.5]
M6	2850	0	BT	10.918	10.769	10.985	11.985	11.911	12.328
M6	2850	-0.5	BT	10.910	10.779	11.009	12.055	11.910	12.329
M7	2650	0	BT	11.742	11.585	11.631	12.354	12.085	12.467
M7	2650	-0.5	BT	11.727	11.592	11.645	12.397	12.084	12.473
M8	2500	0	BT	12.168	12.012	12.022	12.664	12.285	12.651
M8	2500	-0.5	BT	12.147	12.023	12.040	12.726	12.284	12.656
M9	2400	0	SON	12.461	12.205	12.254	13.044	12.502	12.843
M9	2400	-0.5	SON	12.474	12.147	12.149	13.030	12.506	12.851
L0	2250	0	SON	12.706	12.420	12.458	13.404	12.722	13.052
L0	2250	-0.5	SON	12.717	12.342	12.325	13.362	12.725	13.068
L1	2100	0	SON	12.990	12.675	12.665	13.732	12.939	13.270
L1	2100	-0.5	SON	12.998	12.577	12.506	13.643	12.936	13.297
L2	1960	0	SON	13.338	12.999	12.892	13.996	13.141	13.499
L2	1960	-0.5	SON	13.344	12.882	12.719	13.846	13.130	13.534
L3	1830	0	SON	13.748	13.384	13.147	14.198	13.326	13.727
L3	1830	-0.5	SON	13.754	13.255	12.974	14.022	13.309	13.770
L4	1700	0	SON	14.201	13.806	13.421	14.353	13.494	13.954
L4	1700	-0.5	SON	14.204	13.672	13.268	14.214	13.479	14.002
L5	1590	0	SON	14.660	14.224	13.716	14.496	13.656	14.175
L5	1590	-0.5	SON	14.659	14.097	13.600	14.445	13.648	14.220
L6	1490	0	SON	15.090	14.606	14.026	14.659	13.812	14.382
L6	1490	-0.5	SON	15.081	14.494	13.948	14.706	13.813	14.419
L7	1410	0	SON	15.451	14.928	14.339	14.855	13.966	14.568
L7	1410	-0.5	SON	15.434	14.833	14.285	14.962	13.977	14.596
L8	1350	0	SON	15.714	15.176	14.637	15.066	14.124	14.732
L8	1350	-0.5	SON	15.689	15.092	14.590	15.198	14.139	14.751
L9	1300	0	SON	15.865	15.342	14.901	15.273	14.286	14.880
L9	1300	-0.5	SON	15.834	15.267	14.857	15.423	14.305	14.892
T0	1260	0	SON	15.908	15.437	15.134	15.493	14.461	15.014
T0	1260	-0.5	SON	15.871	15.369	15.085	15.647	14.482	15.022
T1	1230	0	SON	15.861	15.485	15.341	15.712	14.655	15.142
T1	1230	-0.5	SON	15.821	15.421	15.289	15.870	14.678	15.147
T2	1200	0	SON	15.765	15.522	15.545	15.958	14.878	15.273
T2	1200	-0.5	SON	15.720	15.463	15.489	16.119	14.903	15.276
T3	1160	0	SON	15.673	15.603	15.780	16.269	15.142	15.417
T3	1160	-0.5	SON	15.623	15.548	15.715	16.433	15.167	15.415
T4	1120	0	SON	15.650	15.783	16.084	16.630	15.459	15.582
T4	1120	-0.5	SON	15.596	15.732	16.010	16.796	15.486	15.577
T5	1050	0	SON	15.773	16.122	16.507	17.131	15.842	15.782
T5	1050	-0.5	SON	15.713	16.077	16.416	17.304	15.870	15.772
T6	960	0	SON	16.116	16.672	17.099	17.780	16.308	16.028
T6	960	-0.5	SON	16.054	16.634	16.982	17.987	16.337	16.011
T7	840	0	SON	16.754	17.472	17.907	18.678	16.874	16.335
T7	840	-0.5	SON	16.702	17.438	17.747	18.891	16.902	16.314

Table 2 continued on next page

**Table 2** (*continued*)

SpT	$T_{eff}$ (K) <sup>a</sup>	[M/H]	Model	F115W	F150W	F200W	F277W	F356W	F444W
	Base magnitude	T8-Y2 <sup>c</sup>		MKO J	2MASS H	2MASS H	IRAC [3.6]	IRAC [3.6]	IRAC [4.5]
T8	700	0	SON	17.393	19.593	20.479	20.010	17.909	16.907
T8	700	-0.5	SON	17.365	19.538	21.128	20.329	17.940	16.881
T9	530	0	SON	18.808	21.234	22.785	21.909	18.772	17.483
T9	530	-0.5	SON	18.851	21.193	23.583	22.095	18.813	17.449
Y0	420	0	SON	20.733	23.561	26.062	23.767	19.687	18.159
Y0	420	-0.5	SON	20.899	23.533	26.853	23.787	19.738	18.121
Y1	350	0	SON	23.362	27.059	30.632	25.362	20.476	18.916
Y1	350	-0.5	SON	23.519	27.048	31.020	25.201	20.541	18.876
Y2	250	0	SON	26.810	32.485	38.047	26.911	20.737	19.743
Y2	250	-0.5	SON	26.356	32.489	37.352	26.796	20.868	19.699

<sup>a</sup>Temperatures estimated from the spectral type/ $T_{eff}$  relation of [Pecaut & Mamajek \(2013\)](#).

<sup>b</sup>Based on the [Dupuy & Liu \(2012\)](#) absolute magnitude/spectral type relations.

<sup>c</sup>Based on the [Kirkpatrick et al. \(2021\)](#) absolute magnitude/spectral type relations.

NOTE—Model references: [BT] BT-Settl models ([Allard et al. 2012](#)); [SON] Sonora-Bobcat models ([Marley et al. 2021](#)).

## REFERENCES

- Aganze, C., Burgasser, A. J., Malkan, M., et al. 2022, *ApJ*, 934, 73, doi: [10.3847/1538-4357/ac7053](https://doi.org/10.3847/1538-4357/ac7053)
- Allard, F., Homeier, D., & Freytag, B. 2012, *Philosophical Transactions of the Royal Society A*, 370, 2765, doi: [10.1098/rsta.2011.0269](https://doi.org/10.1098/rsta.2011.0269)
- Astropy Collaboration, Robitaille, T. P., Tollerud, E. J., et al. 2013, *A&A*, 558, A33, doi: [10.1051/0004-6361/201322068](https://doi.org/10.1051/0004-6361/201322068)
- Astropy Collaboration, Price-Whelan, A. M., Sipőcz, B. M., et al. 2018, *AJ*, 156, 123, doi: [10.3847/1538-3881/aabc4f](https://doi.org/10.3847/1538-3881/aabc4f)
- Astropy Collaboration, Price-Whelan, A. M., Lim, P. L., et al. 2022, *ApJ*, 935, 167, doi: [10.3847/1538-4357/ac7c74](https://doi.org/10.3847/1538-4357/ac7c74)
- Atek, H., Labbé, I., Furtak, L. J., et al. 2023, arXiv e-prints, arXiv:2308.08540, doi: [10.48550/arXiv.2308.08540](https://doi.org/10.48550/arXiv.2308.08540)
- Azzam, A. A. A., Tennyson, J., Yurchenko, S. N., & Naumenko, O. V. 2016, *MNRAS*, 460, 4063, doi: [10.1093/mnras/stw1133](https://doi.org/10.1093/mnras/stw1133)
- Bardalez Gagliuffi, D. C., Burgasser, A. J., Schmidt, S. J., et al. 2019, *ApJ*, 883, 205, doi: [10.3847/1538-4357/ab253d](https://doi.org/10.3847/1538-4357/ab253d)
- Beiler, S. A., Cushing, M. C., Kirkpatrick, J. D., et al. 2023, *ApJL*, 951, L48, doi: [10.3847/2041-8213/ace32c](https://doi.org/10.3847/2041-8213/ace32c)
- Best, W. M. J., Liu, M. C., Magnier, E. A., & Dupuy, T. J. 2020, *AJ*, 159, 257, doi: [10.3847/1538-3881/ab84f4](https://doi.org/10.3847/1538-3881/ab84f4)
- Bezanson, R., Labbe, I., Whitaker, K. E., et al. 2022, arXiv e-prints, arXiv:2212.04026, doi: [10.48550/arXiv.2212.04026](https://doi.org/10.48550/arXiv.2212.04026)
- Brammer, G. 2022, msaexp: NIRSpec analysis tools, 0.3.4, Zenodo, Zenodo, doi: [10.5281/zenodo.7313329](https://doi.org/10.5281/zenodo.7313329)
- Burgasser, A. J. 2004, *ApJS*, 155, 191, doi: [10.1086/424386](https://doi.org/10.1086/424386)
- . 2007, *ApJ*, 659, 655, doi: [10.1086/511027](https://doi.org/10.1086/511027)
- Burgasser, A. J., Burrows, A., & Kirkpatrick, J. D. 2006a, *ApJ*, 639, 1095, doi: [10.1086/499344](https://doi.org/10.1086/499344)
- Burgasser, A. J., Geballe, T. R., Leggett, S. K., Kirkpatrick, J. D., & Golimowski, D. A. 2006b, *ApJ*, 637, 1067, doi: [10.1086/498563](https://doi.org/10.1086/498563)
- Burgasser, A. J., McElwain, M. W., Kirkpatrick, J. D., et al. 2004, *AJ*, 127, 2856, doi: [10.1086/383549](https://doi.org/10.1086/383549)
- Burgasser, A. J., & Splat Development Team. 2017, in *Astronomical Society of India Conference Series*, Vol. 14, Astronomical Society of India Conference Series, 7–12, <https://arxiv.org/abs/1707.00062>
- Burningham, B., Cardoso, C. V., Smith, L., et al. 2013, *MNRAS*, 433, 457, doi: [10.1093/mnras/stt740](https://doi.org/10.1093/mnras/stt740)
- Bushouse, H., Eisenhamer, J., Dencheva, N., et al. 2023, JWST Calibration Pipeline, 1.11.3, Zenodo, doi: [10.5281/zenodo.8157276](https://doi.org/10.5281/zenodo.8157276)
- Carollo, D., Beers, T. C., Lee, Y. S., et al. 2008, *Nature*, 451, 216, doi: [10.1038/nature06542](https://doi.org/10.1038/nature06542)
- Day-Jones, A. C., Marocco, F., Pinfield, D. J., et al. 2013, *MNRAS*, 430, 1171, doi: [10.1093/mnras/sts685](https://doi.org/10.1093/mnras/sts685)
- Dupuy, T. J., & Liu, M. C. 2012, *ApJS*, 201, 19, doi: [10.1088/0067-0049/201/2/19](https://doi.org/10.1088/0067-0049/201/2/19)
- Furtak, L. J., Labbé, I., Zitrin, A., et al. 2023, arXiv e-prints, arXiv:2308.05735, doi: [10.48550/arXiv.2308.05735](https://doi.org/10.48550/arXiv.2308.05735)
- Gerasimov, R., Burgasser, A. J., Homeier, D., et al. 2022, *ApJ*, 930, 24, doi: [10.3847/1538-4357/ac61e5](https://doi.org/10.3847/1538-4357/ac61e5)
- Gerasimov, R., Homeier, D., Burgasser, A., & Bedin, L. R. 2020, *Research Notes of the American Astronomical Society*, 4, 214, doi: [10.3847/2515-5172/abcf2c](https://doi.org/10.3847/2515-5172/abcf2c)
- Gizis, J. E. 1997, *AJ*, 113, 806, doi: [10.1086/118302](https://doi.org/10.1086/118302)
- Glazebrook, K., Nanayakkara, T., Jacobs, C., et al. 2023, *ApJL*, 947, L25, doi: [10.3847/2041-8213/acba8b](https://doi.org/10.3847/2041-8213/acba8b)
- Gonzales, E. C., Burningham, B., Faherty, J. K., et al. 2021, *ApJ*, 923, 19, doi: [10.3847/1538-4357/ac294e](https://doi.org/10.3847/1538-4357/ac294e)

- Goulding, A. D., Greene, J. E., Setton, D. J., et al. 2023, arXiv e-prints, arXiv:2308.02750, doi: [10.48550/arXiv.2308.02750](https://doi.org/10.48550/arXiv.2308.02750)
- Greene, J. E., Labbe, I., Goulding, A. D., et al. 2023, arXiv e-prints, arXiv:2309.05714, doi: [10.48550/arXiv.2309.05714](https://doi.org/10.48550/arXiv.2309.05714)
- Griffith, C. A., & Yelle, R. V. 1999, ApJL, 519, L85, doi: [10.1086/312103](https://doi.org/10.1086/312103)
- Hainline, K. N., Helton, J. M., Johnson, B. D., et al. 2023, arXiv e-prints, arXiv:2309.03250, doi: [10.48550/arXiv.2309.03250](https://doi.org/10.48550/arXiv.2309.03250)
- Hayashi, C., & Nakano, T. 1963, Progress of Theoretical Physics, 30, 460, doi: [10.1143/PTP.30.460](https://doi.org/10.1143/PTP.30.460)
- Hill, C., Yurchenko, S. N., & Tennyson, J. 2013, Icarus, 226, 1673, doi: [10.1016/j.icarus.2012.07.028](https://doi.org/10.1016/j.icarus.2012.07.028)
- Holwerda, B. W., Hsu, C.-C., Hathi, N., et al. 2023, arXiv e-prints, arXiv:2309.05835, doi: [10.48550/arXiv.2309.05835](https://doi.org/10.48550/arXiv.2309.05835)
- Horne, K. 1986, PASP, 98, 609, doi: [10.1086/131801](https://doi.org/10.1086/131801)
- Hsu, C.-C., Burgasser, A. J., Theissen, C. A., et al. 2021, ApJS, 257, 45, doi: [10.3847/1538-4365/ac1c7d](https://doi.org/10.3847/1538-4365/ac1c7d)
- Jurić, M., Ivezić, Ž., Brooks, A., et al. 2008, ApJ, 673, 864, doi: [10.1086/523619](https://doi.org/10.1086/523619)
- Karalidi, T., Marley, M., Fortney, J. J., et al. 2021, ApJ, 923, 269, doi: [10.3847/1538-4357/ac3140](https://doi.org/10.3847/1538-4357/ac3140)
- Kirkpatrick, J. D., Gelino, C. R., Cushing, M. C., et al. 2012, ApJ, 753, 156, doi: [10.1088/0004-637X/753/2/156](https://doi.org/10.1088/0004-637X/753/2/156)
- Kirkpatrick, J. D., Martin, E. C., Smart, R. L., et al. 2019, ApJS, 240, 19, doi: [10.3847/1538-4365/aaf6af](https://doi.org/10.3847/1538-4365/aaf6af)
- Kirkpatrick, J. D., Gelino, C. R., Faherty, J. K., et al. 2021, ApJS, 253, 7, doi: [10.3847/1538-4365/abd107](https://doi.org/10.3847/1538-4365/abd107)
- Kuchner, M. J., Faherty, J. K., Schneider, A. C., et al. 2017, ApJL, 841, L19, doi: [10.3847/2041-8213/aa7200](https://doi.org/10.3847/2041-8213/aa7200)
- Kumar, S. S. 1962, AJ, 67, 579, doi: [10.1086/108658](https://doi.org/10.1086/108658)
- . 1963, ApJ, 137, 1121, doi: [10.1086/147589](https://doi.org/10.1086/147589)
- Labbe, I., Greene, J. E., Bezanson, R., et al. 2023, arXiv e-prints, arXiv:2306.07320, doi: [10.48550/arXiv.2306.07320](https://doi.org/10.48550/arXiv.2306.07320)
- Langeroodi, D., & Hjorth, J. 2023, arXiv e-prints, arXiv:2308.10900, doi: [10.48550/arXiv.2308.10900](https://doi.org/10.48550/arXiv.2308.10900)
- Leggett, S. K., Morley, C. V., Marley, M. S., & Saumon, D. 2015, ApJ, 799, 37, doi: [10.1088/0004-637X/799/1/37](https://doi.org/10.1088/0004-637X/799/1/37)
- Leggett, S. K., Tremblin, P., Saumon, D., et al. 2016, ApJ, 824, 2, doi: [10.3847/0004-637X/824/1/2](https://doi.org/10.3847/0004-637X/824/1/2)
- Li, G., Gordon, I. E., Rothman, L. S., et al. 2015, ApJS, 216, 15, doi: [10.1088/0067-0049/216/1/15](https://doi.org/10.1088/0067-0049/216/1/15)
- Linsky, J. L. 1969, ApJ, 156, 989, doi: [10.1086/150030](https://doi.org/10.1086/150030)
- Lodders, K., & Fegley, B. 2002, Icarus, 155, 393, doi: [10.1006/icar.2001.6740](https://doi.org/10.1006/icar.2001.6740)
- Lodieu, N., Zapatero Osorio, M. R., Martín, E. L., Rebolo López, R., & Gauza, B. 2022, A&A, 663, A84, doi: [10.1051/0004-6361/202243516](https://doi.org/10.1051/0004-6361/202243516)
- Marley, M. S., Saumon, D., Visscher, C., et al. 2021, ApJ, 920, 85, doi: [10.3847/1538-4357/ac141d](https://doi.org/10.3847/1538-4357/ac141d)
- Meisner, A. M., Schneider, A. C., Burgasser, A. J., et al. 2021, ApJ, 915, 120, doi: [10.3847/1538-4357/ac013c](https://doi.org/10.3847/1538-4357/ac013c)
- Miles, B. E., Skemer, A. J. I., Morley, C. V., et al. 2020, AJ, 160, 63, doi: [10.3847/1538-3881/ab9114](https://doi.org/10.3847/1538-3881/ab9114)
- Miles, B. E., Biller, B. A., Patapis, P., et al. 2023, ApJL, 946, L6, doi: [10.3847/2041-8213/acb04a](https://doi.org/10.3847/2041-8213/acb04a)
- Mould, J. R., & McElroy, D. B. 1978, ApJ, 220, 935, doi: [10.1086/155983](https://doi.org/10.1086/155983)
- Noll, K. S., Geballe, T. R., Leggett, S. K., & Marley, M. S. 2000, ApJL, 541, L75, doi: [10.1086/312906](https://doi.org/10.1086/312906)
- Nonino, M., Glazebrook, K., Burgasser, A. J., et al. 2023, ApJL, 942, L29, doi: [10.3847/2041-8213/ac8e5f](https://doi.org/10.3847/2041-8213/ac8e5f)
- Pecaut, M. J., & Mamajek, E. E. 2013, ApJS, 208, 9, doi: [10.1088/0067-0049/208/1/9](https://doi.org/10.1088/0067-0049/208/1/9)



- Phillips, M. W., Tremblin, P., Baraffe, I., et al. 2020, *A&A*, 637, A38, doi: [10.1051/0004-6361/201937381](https://doi.org/10.1051/0004-6361/201937381)
- Polyansky, O. L., Kyuberis, A. A., Zobov, N. F., et al. 2018, *MNRAS*, 480, 2597, doi: [10.1093/mnras/sty1877](https://doi.org/10.1093/mnras/sty1877)
- Reid, I. N., Kirkpatrick, J. D., Liebert, J., et al. 1999, *ApJ*, 521, 613, doi: [10.1086/307589](https://doi.org/10.1086/307589)
- Reyl  , C., Jardine, K., Fouqu  , P., et al. 2021, *A&A*, 650, A201, doi: [10.1051/0004-6361/202140985](https://doi.org/10.1051/0004-6361/202140985)
- Ryan, R. E., J., & Reid, I. N. 2016, *AJ*, 151, 92, doi: [10.3847/0004-6256/151/4/92](https://doi.org/10.3847/0004-6256/151/4/92)
- Ryan, R. E., Thorman, P., Aganze, C., et al. 2022, *ApJ*, 932, 96, doi: [10.3847/1538-4357/ac6de5](https://doi.org/10.3847/1538-4357/ac6de5)
- Sanghi, A., Liu, M. C., Best, W. M., et al. 2023, *Research Notes of the American Astronomical Society*, 7, 194, doi: [10.3847/2515-5172/acf864](https://doi.org/10.3847/2515-5172/acf864)
- Saumon, D., Marley, M. S., Cushing, M. C., et al. 2006, *ApJ*, 647, 552, doi: [10.1086/505419](https://doi.org/10.1086/505419)
- Schneider, A. C., Burgasser, A. J., Gerasimov, R., et al. 2020, *ApJ*, 898, 77, doi: [10.3847/1538-4357/ab9a40](https://doi.org/10.3847/1538-4357/ab9a40)
- Sorahana, S., & Yamamura, I. 2012, *ApJ*, 760, 151, doi: [10.1088/0004-637X/760/2/151](https://doi.org/10.1088/0004-637X/760/2/151)
- Sousa-Silva, C., Al-Refaie, A. F., Tennyson, J., & Yurchenko, S. N. 2015, *MNRAS*, 446, 2337, doi: [10.1093/mnras/stu2246](https://doi.org/10.1093/mnras/stu2246)
- Stauffer, J. R., Schultz, G., & Kirkpatrick, J. D. 1998, *ApJL*, 499, L199+, doi: [10.1086/311379](https://doi.org/10.1086/311379)
- Tennyson, J., & Yurchenko, S. N. 2012, *MNRAS*, 425, 21, doi: [10.1111/j.1365-2966.2012.21440.x](https://doi.org/10.1111/j.1365-2966.2012.21440.x)
- van Vledder, I., van der Vlugt, D., Holwerda, B. W., et al. 2016, *MNRAS*, 458, 425, doi: [10.1093/mnras/stw258](https://doi.org/10.1093/mnras/stw258)
- Visscher, C., Lodders, K., & Fegley, B. J. 2006, *ApJ*, 648, 1181, doi: [10.1086/506245](https://doi.org/10.1086/506245)
- Wang, B., Fujimoto, S., Labbe, I., et al. 2023a, arXiv e-prints, arXiv:2308.03745, doi: [10.48550/arXiv.2308.03745](https://doi.org/10.48550/arXiv.2308.03745)
- Wang, P.-Y., Goto, T., Ho, S. C. C., et al. 2023b, *MNRAS*, 523, 4534, doi: [10.1093/mnras/stad1679](https://doi.org/10.1093/mnras/stad1679)
- Weaver, J. R., Cutler, S. E., Pan, R., et al. 2023, arXiv e-prints, arXiv:2301.02671, doi: [10.48550/arXiv.2301.02671](https://doi.org/10.48550/arXiv.2301.02671)
- Yamamura, I., Tsuji, T., & Tanab  , T. 2010, *ApJ*, 722, 682, doi: [10.1088/0004-637X/722/1/682](https://doi.org/10.1088/0004-637X/722/1/682)
- Yurchenko, S. N., Barber, R. J., & Tennyson, J. 2011, *MNRAS*, 413, 1828, doi: [10.1111/j.1365-2966.2011.18261.x](https://doi.org/10.1111/j.1365-2966.2011.18261.x)
- Yurchenko, S. N., Mellor, T. M., Freedman, R. S., & Tennyson, J. 2020, *MNRAS*, 496, 5282, doi: [10.1093/mnras/staa1874](https://doi.org/10.1093/mnras/staa1874)
- Zhang, S., Luo, A. L., Comte, G., et al. 2019a, *ApJS*, 240, 31, doi: [10.3847/1538-4365/aafb32](https://doi.org/10.3847/1538-4365/aafb32)
- Zhang, Z. H., Burgasser, A. J., G  lvez-Ortiz, M. C., et al. 2019b, *MNRAS*, 486, 1260, doi: [10.1093/mnras/stz777](https://doi.org/10.1093/mnras/stz777)